Submitted to **Computers and Geotechnics**

May 08, 2016

Three-Dimensional Slope Reliability and Risk Assessment Using Auxiliary Random Finite Element Method

Te Xiao, Dian-Qing Li*, Zi-Jun Cao

State Key Laboratory of Water Resources and Hydropower Engineering Science, Wuhan University, 8 Donghu South Road, Wuhan 430072, P. R. China.

Siu-Kui Au

Institute for Risk and Uncertainty, University of Liverpool, Harrison Hughes Building, Brownlow Hill, Liverpool, L69 3GH, United Kingdom.

Kok-Kwang Phoon

Department of Civil and Environmental Engineering, National University of Singapore, Blk E1A, #07-03, 1 Engineering Drive 2, Singapore 117576, Singapore.

*Corresponding author

State Key Laboratory of Water Resources and Hydropower Engineering Science, Wuhan University, 8 Donghu South Road, Wuhan 430072, P. R. China.

Tel: (86)-27-6877 2496

Fax: (86)-27-6877 4295

E-mail: dianqing@whu.edu.cn

7800 words, 2 tables and 11 figures

Abstract:

This paper aims to propose an auxiliary random finite element method (ARFEM) for efficient three-dimensional (3-D) slope reliability analysis and risk assessment considering spatial variability of soil properties. The ARFEM mainly consists of two steps: (1) preliminary analysis using a relatively coarse finite-element model and Subset Simulation, and (2) target analysis using a detailed finite-element model and response conditioning method. The 3-D spatial variability of soil properties is explicitly modeled using the expansion optimal linear estimation approach. A 3-D soil slope example is presented to demonstrate the validity of ARFEM. Finally, a sensitivity study is carried out to explore the effect of horizontal spatial variability. The results indicate that the proposed ARFEM not only provides reasonably accurate estimates of slope failure probability and risk, but also significantly reduces the computational effort at small probability levels. 3-D slope probabilistic analysis (including both 3-D slope stability analysis and 3-D spatial variability modelling) can reflect slope failure mechanism more realistically in terms of the shape, location and length of slip surface. Horizontal spatial variability can significantly influence the failure mode, reliability and risk of 3-D slopes, especially for long slopes with relatively strong horizontal spatial variability. These effects can be properly incorporated into 3-D slope reliability analysis and risk assessment using ARFEM.

Keywords: Slope stability; Reliability analysis; Risk assessment; Spatial variability; Random finite element method; Response conditioning method

1 Introduction

Slope failure (e.g., landslides) is one of the major natural hazards in the world. The occurrence probability and risk of slope failure are related to various geotechnical uncertainties (e.g., Li et al., 2011, 2015c, 2016d; Tang et al., 2013, 2015; Phoon and Ching, 2014; Le, 2014; Jiang et al., 2014; Chen et al., 2016; Kasama and Whittle, 2016), among which spatial variability of soil properties is one of the most significant uncertainties affecting slope reliability and risk. Previous studies on slope reliability analysis and risk assessment that account for spatial variability mainly focus on two-dimensional (2-D) analysis, such as Griffiths and Fenton (2004), Santoso et al. (2011), Wang et al. (2011), Huang et al. (2013), Zhu et al. (2013), Li et al. (2014a,b, 2015a, 2016c), Jamshidi Chenari and Alaie (2015). As shown in Fig. 1, 2-D analysis implicitly assumes infinite length of slope and perfect correlation of soil properties (i.e., infinite spatial autocorrelation distance) in the axial direction. Based on these assumptions, slopes fail along columnar slip surface with infinite length in three-dimensional (3-D) space. This is inconsistent with the actual failure surfaces observed in slope engineering, where slope may fail at any locations of the slope with an irregular and finite slip surface. Thus, it is necessary to investigate 3-D slope reliability analysis and risk assessment, particularly with both 3-D slope stability analysis and 3-D spatial variability modeling of soil properties.

Several studies (e.g., Vanmarcke, 1977, 2011; Griffiths et al., 2009; Hicks and Spencer, 2010; Ji, 2014; Ji and Chan, 2014) have made attempts to assess 3-D slope reliability. These studies can be classified into three categories according to the adopted reliability methods:

first-order second-moment method (FOSM), first-order reliability method (FORM), and Monte Carlo Simulation (MCS). Vanmarcke (1977, 2011) pioneered analytical 3-D slope reliability analysis using FOSM and considered the problem as an extension of 2-D slope reliability analysis based on local average and first-passage theories. This work is elegant and valuable. However, it assumed that slope fails along several prescribed cylindrical slip surfaces, which may lead to an overestimated slope reliability since many other potential slip surfaces (e.g., non-cylindrical ones) are ignored. By only accounting for the axial spatial variability, FORM was also applied to 3-D slope reliability analysis (Ji, 2014; Ji and Chan, 2014). If 3-D spatial variability in axial, lateral and vertical directions as shown in Fig. 1 are completely taken into consideration, FORM may encounter computational difficulties, such as high-dimensional problem (Schuëller et al., 2004).

Compared with FOSM and FORM, MCS is the most widely-used reliability method for 3-D slope reliability analysis, thanks to the development of random finite element method (RFEM) (Griffiths and Fenton, 2004). The original RFEM, also referred as MCS-based RFEM, incorporates the spatial variability of soil properties into slope reliability analysis using finite-element (FE) analysis and MCS. There are several successful applications of RFEM in reliability analysis of 3-D slope (e.g., Griffiths et al., 2009; Hicks and Spencer, 2010; Hicks et al., 2014; Li et al., 2015b) and slope risk assessment (e.g., Huang et al., 2013; Li et al., 2016a). RFEM is a rigorous approach since the FE analysis of slope stability can automatically locate the critical slip surface without assumptions on the shape and location. Nevertheless, MCS-based RFEM usually requires intensive computational efforts (Ji and Low,

43 2012), particularly for detailed 3-D FE models and small probability levels (e.g., slope failure
44 probability $P_f < 10^{-3}$). One simple strategy to address this problem is to adopt a relatively
45 coarse FE model (e.g., the model with coarse FE mesh) in RFEM to improve the
46 computational efficiency of deterministic slope stability analysis. However, coarse FE model
47 may not produce accurate results compared to detailed FE model (e.g., the model with fine
48 FE mesh). For this reason, another RFEM run with detailed FE model is still requisite if more
49 accurate results are required, for example, at later design stages. The computational effort
50 paid for the coarse FE model-based RFEM is thus wasted, and it cannot facilitate the detailed
51 FE model-based RFEM neither, because of no interaction between the two RFEM runs.

52 In addition, previous studies based on 2-D analysis indicated that the horizontal spatial
53 variability (i.e., lateral spatial variability in the 3-D perspective, see Fig. 1) has minimal
54 influence on slope reliability (e.g., Jiang et al., 2015; Xiao et al., 2015). One possible reason
55 is that the lateral scale of slopes is almost in the same order of magnitude as the horizontal
56 autocorrelation distance, namely 20m ~ 40m (Phoon and Kulhawy, 1999). In this case, the
57 effect of horizontal spatial variability cannot be captured in 2-D slope reliability analysis. For
58 3-D slopes, the axial scale can be much larger than the horizontal autocorrelation distance.
59 The effect of horizontal spatial variability on 3-D slope reliability and risk has not been
60 explored systematically.

61 This paper aims to propose an auxiliary random finite element method (ARFEM) for
62 efficient 3-D slope reliability analysis and risk assessment, and explore the effect of
63 horizontal spatial variability on 3-D slopes. To achieve these goals, the paper is organized as

64 below. In Section 2, the ARFEM is developed. In Section 3, the modeling of 3-D spatially
65 variable soil properties is presented. The computational effort of ARFEM is discussed in
66 Section 4 and the implementation procedure of ARFEM is summarized in Section 5. A 3-D
67 soil slope example is then presented in Section 6 to demonstrate the validity of ARFEM.
68 Finally, a sensitivity study is carried out to explore the effect of horizontal spatial variability
69 on 3-D slope reliability and risk in Section 7.

70 **2 Auxiliary random finite element method**

71 In slope reliability analysis and risk assessment, the probability of slope failure, P_f, is defined
72 as the probability that the safety factor of slope stability, FS, is smaller than a given threshold
73 fs (e.g., $fs = 1$), namely $P_f = P(FS < fs)$, and the slope failure risk, R, can be defined as the
74 product of P_f and the average failure consequence $\bar{C}$ (Huang et al., 2013; Li et al., 2016a).
75 The computational efficiency and accuracy of P_f and R depend on the deterministic analysis
76 model of slope stability, such as the FE models with coarse and fine FE meshes (referred as
77 coarse and fine FE models, respectively). Both of these two FE models are adopted in
78 ARFEM, which, in turn, constitute two major steps of ARFEM: (1) preliminary analysis
79 using a relatively coarse FE model and Subset Simulation (SS) (Au and Beck, 2001), and (2)
80 target analysis using a fine FE model and response conditioning method (RCM) (Au, 2007).
81 They are provided in the following two subsections. To facilitate understanding, subscripts
82 "p" and "t" shall denote the estimates obtained from preliminary and target analyses of
83 ARFEM, respectively.

84 **2.1 Preliminary analysis using coarse FE model and SS**

Preliminary analysis aims to efficiently assess slope reliability and risk. For this purpose, coarse FE model and SS are adopted to perform deterministic slope stability analysis and slope reliability analysis at small probability levels, respectively. SS (Au and Beck, 2001; Au and Wang, 2014) stems from the idea that a small failure probability can be expressed as a product of larger conditional failure probabilities for some intermediate failure events, thereby converting a rare event simulation problem into a sequence of more frequent ones. Let $fs_1 > fs_2 > \ldots > fs_{m-1} > fs > fs_m$ be a decreasing sequence of intermediate threshold values, and $F_{p,k} = \{FS_p < fs_k, k = 1, 2, \ldots, m\}$ be the intermediate failure events. In implementation, fs_k ($k = 1, 2, \ldots, m$) are determined adaptively so that the estimates of $P(F_{p,1})$ and $P(F_{p,k}|F_{p,k-1})$, $k = 2, 3, \ldots, m$, always correspond to a common specified value of conditional probability p_0. An SS run with m simulation levels (including one direct MCS level and $m-1$ levels of Markov Chain MCS) and N samples in each level results in $mN(1-p_0)+Np_0$ samples in total.

During SS, the sample space is divided into $m+1$ mutually exclusive and collectively exhaustive subsets Ω_k, $k = 0, 1, \ldots, m$, by intermediate threshold values, i.e., $fs_1, fs_2, \ldots, fs_m$, where $\Omega_0 = \{FS_p \geq fs_1\}$, $\Omega_k = \{fs_{k+1} \leq FS_p < fs_k\}$, $k = 1, 2, \ldots, m-1$, and $\Omega_m = \{FS_p < fs_m\}$. Using the Theorem of Total Probability (Ang and Tang, 2007), the $P_{f,p}$ estimated from preliminary analysis can be expressed as

$$P_{f,p} = \sum_{k=0}^{m} P\left(F_p \middle| \Omega_k\right) P\left(\Omega_k\right) = \sum_{k=0}^{m} \sum_{j=1}^{N_k} I_{p,kj} \frac{P\left(\Omega_k\right)}{N_k} \quad (1)$$

where $P(F_p|\Omega_k)$ is the conditional preliminary failure probability given sampling in Ω_k, which can be estimated by $\sum_{j=1}^{N_k} I_{p,kj} \Big/ N_k$; $I_{p,kj} = I(FS_{p,j} < fs|\Omega_k)$ is the indicator function of slope

failure for j-th sample in Ω_k using coarse FE model; $I_{p,kj} = 1$ if the corresponding FS of j-th sample $FS_{p,j} < fs$, otherwise, $I_{p,kj} = 0$; N_k is the number of random samples falling into Ω_k, and it is equal to $N(1-p_0)$ for $k = 0, 1, \ldots, m-1$, and Np_0 for $k = m$; $P(\Omega_k)$ is the occurrence probability of Ω_k, and it is taken as $p_0^k(1-p_0)$ for $k = 0, 1, \ldots, m-1$, and p_0^k for $k = m$ (Wang et al., 2010). In this study, the FS of slope stability is calculated using the shear strength reduction technique (Griffiths and Lane, 1999).

In the context of slope risk assessment, slope failure consequence, C, for each sample should be determined. As pointed out by Huang et al. (2013), slope failure consequence depends on the sliding mass volume, V, which can be taken as an equivalent index to quantify the slope failure consequence for simplicity. Analogous to the estimation of $P_{f,p}$, slope failure risk, R_p, in preliminary analysis can also be estimated as

$$R_p = \sum_{k=0}^{m}\sum_{j=1}^{N_k} C_{p,kj}\frac{P(\Omega_k)}{N_k} = \sum_{k=0}^{m}\sum_{j=1}^{N_k} I_{p,kj}V_{p,kj}\frac{P(\Omega_k)}{N_k} \quad (2)$$

where $C_{p,kj}$ and $V_{p,kj}$ are the failure consequence and sliding mass volume corresponding to j-th sample in Ω_k based on coarse FE model, respectively. It can be proved (Li et al., 2016a) that Eq. (2) is equal to the conventional definition of R, namely, $R = P_f \times \overline{C}$. Herein, failure consequence is evaluated by $C_{p,kj} = I_{p,kj} \times V_{p,kj}$ because it is associated with the occurrence of slope failure. Specifically, failure consequence is represented by the sliding mass volume if slope fails (i.e., $I_{p,kj} = 1$); otherwise, no failure consequence should be considered. In this study, the sliding mass is identified by k-means clustering method (Huang et al., 2013) based on the node displacements obtained from the FE analysis. In addition to V, the sliding mass length, L, is also taken into consideration to investigate the slope failure mechanism. If there

127 is only one sliding mass along the axis of slope, L is defined as the maximum axial length of
128 the sliding mass; otherwise, L is estimated as the sum of axial lengths of all sliding masses,
129 which might occur when the axial spatial variability of soil properties is strong.

130 Although $P_{f,p}$ and R_p obtained using coarse FE model are approximate, preliminary
131 analysis can be finished with acceptable computational effort in practice and provides
132 valuable information and insights (e.g., Ω_k, k = 0, 1, …, m, and random samples in these
133 subsets) for understanding the slope stability problem. How to incorporate such information
134 and insights into the more realistic fine FE model-based reliability analysis has not been
135 explored in the literature. RCM (Au, 2007) opens up a possibility to link these two types of
136 reliability analyses. It is adopted in ARFEM to incorporate the information generated from
137 the coarse FE model-based preliminary analysis into the fine FE model-based target analysis,
138 so as to obtain the refined and consistent estimates of P_f and R efficiently.

139 **2.2 Target analysis using fine FE model and RCM**

140 RCM makes use of the information (i.e., random samples in different subsets) about the
141 problem generated using an approximate solution (e.g., the coarse FE analysis) to achieve
142 efficient and consistent reliability estimates with an accurate solution (e.g., the detailed FE
143 analysis). Note that samples in their close neighborhood will have similar performances
144 (Pradlwarter and Schuëller, 2010). Taking advantage of this property, it is reasonable to select
145 a part of samples as the representative samples in small sample space, which is referred as the
146 sub-binning strategy in RCM (Au, 2007). By this way, Ω_k can be further divided into N_s
147 sub-bins Ω_{kj}, j = 1, 2, …, N_s, which are ranked in a descending order according to FS_p values

estimated from preliminary analysis and have the same number of random samples. In each Ω_{kj}, one of N_k/N_s samples is randomly selected as the representative sample to judge whether Ω_{kj} belongs target failure domain or not, as shown in Fig. 2 schematically. Since Ω_{kj}, j = 1, 2, …, N_s, are mutually exclusive and collectively exhaustive sub-bins of Ω_k, the target slope failure probability, $P_{f,t}$, can be expressed as

$$P_{f,t} = \sum_{k=0}^{m} P\left(F_t|\Omega_k\right)P\left(\Omega_k\right) = \sum_{k=0}^{m}\sum_{j=1}^{N_s} P\left(F_t|\Omega_{kj}\right)P\left(\Omega_{kj}\right) = \sum_{k=0}^{m}\sum_{j=1}^{N_s} I_{t,kj}\frac{P\left(\Omega_k\right)}{N_s} \tag{3}$$

where $P(\Omega_{kj}) = P(\Omega_k)/N_s$ due to the equal division; $P(F_t|\Omega_k)$ and $P(F_t|\Omega_{kj})$ are conditional target failure probabilities given sampling in Ω_k and Ω_{kj}, respectively; $P(F_t|\Omega_{kj})$ can be estimated by $I_{t,kj} = I(FS_t < fs|\Omega_{kj})$, which is the indicator function of slope failure for the representative sample in Ω_{kj} using fine FE model; $I_{t,kj}$ = 1 if the corresponding $FS_t < fs$, otherwise, $I_{t,kj}$ = 0. Similarly, the target slope failure risk, R_t, can be written as

$$R_t = \sum_{k=0}^{m}\sum_{j=1}^{N_s} C_{t,kj}\frac{P\left(\Omega_k\right)}{N_s} = \sum_{k=0}^{m}\sum_{j=1}^{N_s} I_{t,kj}V_{t,kj}\frac{P\left(\Omega_k\right)}{N_s} \tag{4}$$

where $C_{t,kj}$ and $V_{t,kj}$ are the failure consequence and sliding mass volume corresponding to the representative sample in Ω_{kj} based on fine FE model, respectively.

Note that Eqs. (3) and (4) are respective analogues of Eqs. (1) and (2). Using the sub-binning strategy, only $(m+1)N_s$ fine FE analyses are required for estimating $P_{f,t}$ and R_t in Eqs. (3) and (4). This number is much smaller than that (i.e., $mN(1-p_0)+Np_0$) required for directly performing SS based on fine FE model. The computational effort is substantially reduced by incorporating the information generated using SS and coarse FE model in preliminary analysis. It can be shown that the estimates are asymptotically unbiased (Au,

2007). This means the results (i.e., $P_{f,t}$ and R_t) obtained from target analysis of ARFEM converge to those obtained from directly performing MCS or SS based on fine FE model.

2.3 Statistical analysis, CDF, and CRF

This subsection makes use of the random samples to evaluate the statistics of FE responses (i.e., *FS*, *V* and *L*) in ARFEM, among which the mean and variance are of great interest to engineers. Since the samples fall in different sample space with different probability weights, the mean and variance should be evaluated using a weighted summation. Let X denote the FE response (e.g., *FS*, *V* and *L*). The mean, $E(X)$, and variance, $D(X)$, of X can be expressed as

$$E(X) = \sum_{i=1}^{n} X_i w_i \Big/ \sum_{i=1}^{n} w_i \tag{5a}$$

$$D(X) = \sum_{i=1}^{n} X_i^2 w_i \Big/ \sum_{i=1}^{n} w_i - \left[E(X)\right]^2 \tag{5b}$$

where w_i is the probability weight of i-th selected sample, which is taken as $P(\Omega_k)/N_k$ and $P(\Omega_k)/N_s$ for samples in Ω_k in preliminary and target analyses, respectively; n is the number of samples used in analysis. If the statistical analysis is performed on the whole sample space, n is the total sample size (i.e., $mN(1-p_0)+Np_0$ in preliminary analysis and $(m+1)N_s$ in target analysis), and $\sum_{i=1}^{n} w_i = 1$. If it is performed on the failure space only, n is the failure samples size (i.e., $n_{f,p}$ and $n_{f,t}$ for preliminary and target analyses, respectively), and $\sum_{i=1}^{n} w_i$ is then equal to $P_{f,p}$ for preliminary analysis and $P_{f,t}$ for target analysis.

Likewise, P_f and R (see Eqs. (1) – (4)) can also be considered as the weighted summation of the indicator function of slope failure and the failure consequence, respectively, over the whole sample space. Although samples used in ARFEM are generated according to a

predefined fs (e.g., fs = 1), they can be used for evaluating P_f and R at any fs values without additional calculation. It only needs to determine the failure samples according to different fs values and update the indicator functions of slope failure in Eqs. (1) – (4). The variation of P_f as a function of fs can be described by the cumulative distribution function (CDF) of FS. Similarly, an analogue of CDF for slope risk assessment is defined in this work, namely the cumulative risk function (CRF) of FS, which describes the variation of R as a function of fs. The CDF and CRF reflect the slope failure probability and risk at different safety levels. This will be further demonstrated through the illustrative example later.

As mentioned previously, $mN(1-p_0)+Np_0$ random samples are generated in preliminary analysis and $(m+1)N_s$ of them are selected for target analysis. This necessitates the same sample space in the two analyses so that random samples generated in preliminary analysis can be directly used in target analysis. When the spatial variability is considered in FE analysis, it can be modeled as a random field (Vanmarcke, 2010). The random field is usually discretized according to the FE mesh to obtain values of soil properties in each element for the FE analysis, e.g., mid-point method (Li et al., 2016a,b) and local average subdivision method (Griffiths et al., 2009; Hicks and Spencer, 2010). Hence, the random field realized in a coarse FE mesh has less random variables than those generated in a fine FE mesh. This renders difficulty in using random samples, which are generated during preliminary analysis, in target analysis. To address this problem, expansion optimal linear estimation (EOLE) approach (Li and Der Kiureghian, 1993) is adopted in ARFEM for 3-D spatial variability modeling, which is briefly introduced in the following section.

3 EOLE for 3-D spatial variability modeling

EOLE (Li and Der Kiureghian, 1993; Sudret and Der Kiureghian, 2000; Vorechovsky, 2008) is adopted in ARFEM for the following two reasons: (1) the random field realization at the location of the FE mesh can be estimated according to the random field grid, which makes it possible to employ a set of random field grid that differs from the FE mesh; (2) EOLE is computationally efficient and can be easily extended from 2-D to 3-D (Sudret and Der Kiureghian, 2000). In the context of EOLE, a stationary lognormal random field, $S(x)$, of the uncertain soil parameter S (e.g., undrained shear strength, S_u) can be written as

$$S(x) = \exp\left[\mu + \sum_{i=1}^{r} \frac{\zeta_i}{\sqrt{\lambda_i}} \Phi_i^T \Sigma_{x\chi}\right] \tag{6}$$

where x and χ are the coordinates in FE mesh and random field grid, respectively; μ is the mean value of $\ln(S)$; $\boldsymbol{\zeta} = [\zeta_1, \zeta_2, \ldots, \zeta_r]^{\mathrm{T}}$ is a standard normal random vector with independent components; r is the number of truncated terms, which is determined by the required accuracy of random field discretization (e.g., Vorechovsky, 2008); λ_i and Φ_i ($i = 1, 2, \ldots, r$) are the respective eigenvalues and eigenvectors of the covariance matrix of $\ln(S)$ associated with random field grid, i.e., $\Sigma_{\chi\chi}\Phi_i = \lambda_i\Phi_i$; $\Sigma_{x\chi}$ is the optimal linear estimation matrix linking the FE mesh to the random field grid. The autocorrelation coefficients, ρ, in $\Sigma_{\chi\chi}$ and $\Sigma_{x\chi}$ can be calculated from a prescribed autocorrelation function. Consider, for example, the squared exponential autocorrelation function, by which ρ is calculated as

$$\rho = \exp\left[-\left(\frac{\Delta x}{l_h}\right)^2 - \left(\frac{\Delta y}{l_v}\right)^2 - \left(\frac{\Delta z}{l_h}\right)^2\right] \tag{7}$$

where Δx, Δy and Δz are the lateral, vertical and axial distances between two different

229 locations, respectively (see Fig. 1); l_h and l_v are the horizontal and vertical autocorrelation
230 distances, respectively. Eq. (7) assumes that the horizontal spatial variability is isotropic in
231 the lateral and axial directions.

232 Figure 3 shows an example of a random field realization for different FE meshes using
233 EOLE. The random field is first generated on the random field grid as shown in Fig. 3(a)
234 which is determined according to the accuracy of random field mapping, e.g., two points
235 within an autocorrelation distance (Sudret and Der Kiureghian, 2000). The random field
236 realization is then mapped onto three different FE meshes (Figs. 3(b) – 3(d)). The number of
237 random variables remains unchanged during the random field mapping, thus not relying on
238 the FE mesh. This property of EOLE is pivotal for the success of ARFEM.

239 **4 Computational effort of ARFEM**

240 The computational effort of ARFEM consists of two parts. The first part is for the evaluation
241 of $mN(1-p_0)+Np_0$ coarse FE analyses in preliminary analysis, and the second part is for the
242 evaluation of $(m+1)N_s$ fine FE analyses in target analysis. Let ξ denote the ratio of the
243 computational effort using coarse FE model over that using fine FE model. The total
244 computational effort of ARFEM can be expressed in terms of the equivalent number, N_T, of
245 3-D slope stability analysis using fine FE model as follow

246 $$N_T = (m+1)N_s + \xi\left[mN(1-p_0) + Np_0\right] \tag{8}$$

247 The value of ξ depends on the FE models adopted in the calculation. When ξ is relatively
248 small, which means that the coarse FE analysis is much more efficient than the fine FE
249 analysis, the computational effort of ARFEM mainly comes from that used for $(m+1)N_s$ fine

FE analyses in target analysis, which relies on N_s. Typically, N_s is small compared with N.

To further improve the efficiency, parallel computing strategy can be introduced into ARFEM for both deterministic 3-D FE analysis and uncertainty propagation (i.e., SS and RCM). Although the computational efforts of parallel computing and serial computing are equal in terms of sample size, parallel computing can reduce computational time because more computational power is utilized simultaneously. Samples from different Markov Chains (i.e., Np_0) can be parallelized for SS, and all selected samples (i.e., $(m+1)N_s$) can be parallelized for RCM because they have been determined before the target analysis.

5 Implementation procedure

Figure 4 shows the implementation procedure of ARFEM for 3-D slope reliability analysis and risk assessment. The procedure mainly consists of five steps:

(1) Determine statistics (e.g., mean, standard deviation, and autocorrelation distance), autocorrelation function and probability distribution of soil properties, and characterize slope geometry.

(2) Perform preliminary analysis using SS with coarse FE model, during which $mN(1-p_0)+Np_0$ random samples are generated and Ω_k (k = 0, 1, …, m) are progressively determined based on the FS_p values. The results of slope reliability and risk (i.e., P_{fsp} and R_p) are calculated using Eqs. (1) and (2), respectively.

(3) Divide Ω_k (k = 0, 1, …, m) into N_s equal sub-bins Ω_{kj} (j = 1, 2, …, N_s). In each Ω_{kj}, one sample is selected randomly, leading to a total of $(m+1)N_s$ selected samples.

(4) Perform target analysis using RCM with fine FE model and the $(m+1)N_s$ samples selected

in Step (3). The results of slope reliability and risk (i.e., $P_{f,t}$ and R_t) are refined using Eqs. (3) and (4), respectively.

(5) Carry out statistical analyses on FE responses using Eq. (5) to obtain their respective statistics.

Although the abovementioned implementation procedure is somewhat more complicated and non-straightforward than MCS-based RFEM, ARFEM can be developed as a user-friendly toolbox and be implemented in a non-intrusive manner (Li et al., 2016a,b). By this means, the deterministic slope stability analysis is deliberately decoupled from the uncertainty modeling and propagation. A thorough understanding of ARFEM is always advantageous but not a prerequisite for engineers to use the toolbox. They only need to focus on the deterministic slope stability analysis that they are more familiar with, i.e., developing the coarse and fine FE models for 3-D slope stability analysis in commercial FE software packages (e.g., Abaqus (Dassault Systèmes, 2015)). The toolbox will repeatedly invoke the FE models to calculate *FS* using the shear strength reduction technique and to evaluate *V* and *L* based on sliding mass identification, and will return the preliminary and target results of slope reliability and risk as outputs. This facilitates the practical application of ARFEM in slope reliability and risk assessment.

6 Illustrative example

For illustration, this section applies ARFEM to evaluate the failure probability and risk of a 3-D soil slope. As shown in Fig. 5, the slope has a height (H) of 6m, a slope angle (α) of about 26.6°, and a length (B) of 100m. Two FE models are developed in Abaqus, as shown in

292 Fig. 6. The FE mesh size measures 2m×2m×5m for the coarse FE model and 1m×1m×1m for
293 the fine one. In both models, the bottom (y = 0m), front (z = 100m) and back (z = 0m) sides
294 of slope are fully fixed, and the left (x = 0m) and right (x = 40m) sides are constrained by
295 vertical rollers. For soil property, the elastic-perfectly plastic constitutive model with
296 Mohr-Coulomb failure criterion is used in both FE analyses.

297 Undrained shear strength, S_u, is considered to be lognormally distributed with mean of
298 30kPa and coefficient of variation (COV) of 0.3. The spatial variability of S_u is modeled
299 using the squared exponential autocorrelation function with horizontal and vertical
300 autocorrelation distances of 20m and 2m, respectively. More actual information on spatial
301 variability of soil properties can be inferred from the site investigation (e.g., Cao and Wang,
302 2014; Lloret-Cabot et al., 2014; Ching and Wang, 2016; Cao et al., 2016; Wang et al., 2016).
303 The unit weight, Young's modulus and Poisson's ratio of soil are 20kN/m^3, 100MPa and 0.3,
304 respectively. Note that, the Poisson's ratio has minimal influence on the calculated FS in
305 slope stability analysis as pointed out by Griffiths and Lane (1999) and Griffiths and Marquez
306 (2007). Although a value of approximately 0.5 for the Poisson's ratio in undrained condition
307 would be most appropriate, a value of 0.3 is adopted in this study, which is commonly used in
308 RFEM-based probabilistic slope stability analysis (e.g., Hicks and Spencer, 2010; Hicks et al.,
309 2014; Li et al., 2015b).

310 Figure 6 shows the results of deterministic slope stability analysis based on the mean
311 value of S_u. The failure modes (i.e., critical slip surfaces) identified by the two models are
312 similar and nearly cylindrical. Their sliding mass lengths are almost the same as the slope

313 length. These results appear to be similar to those of 2-D analysis, namely, sliding along the
314 whole slope length from the 3-D perspective. This is because the slope is relatively long and
315 soil is homogeneous without considering spatial variability, which basically satisfies the
316 assumptions adopted in 2-D analysis. The *FS*, *V* and *L* calculated by the coarse FE model are
317 1.651, 7030m^3 and 85m, respectively, while they are 1.593, 9068m^3 and 91m for the fine FE
318 model, respectively. The coarse FE model slightly overestimates *FS*, which is consistent with
319 the observation reported by Griffiths and Marquez (2007), and underestimates *V* and *L*. This
320 may lead to unconservative estimates of P_f and *R* in probabilistic slope stability analysis.
321 Since the coarse FE model is much more efficient than the fine FE model (i.e., 48s vs. 35min),
322 they are adopted to perform preliminary and target analyses in ARFEM, respectively.

323 **6.1 Comparison between 2-D and 3-D slope stability analyses**

324 As can be seen from the above results, the failure mechanism of a 3-D homogeneous slope is
325 similar to that of a 2-D slope. However, soils are typically heterogeneous in geotechnical
326 practice, which can be partially described by spatial variability. Taking this into consideration,
327 this subsection compares 2-D and 3-D slope stability analyses in spatially variable soils.

328 A typical random field realization of the slope is shown in Fig. 7(a). The corresponding
329 *FS* of 3-D slope stability analysis calculated by the fine FE model is 0.741, which implies the
330 slope fails. Its slip surface is nearly spherical with a small sliding mass length (i.e., 24m)
331 located from 19.5m to 43.5m in the axial direction. The 3-D heterogeneous slope considering
332 spatial variability of soil properties models real slope failure event more realistically than the
333 3-D homogeneous slope in terms of the shape, location and length of slip surface. A series

334 (i.e., 100) of cross sections are extracted from the 3-D realization to perform 2-D FE analyses.
335 As shown in Fig. 7, the 2-D *FS* values and slip surfaces vary along the axis of slope. The
336 location of the failed cross sections is from 10.5m to 48.5m, whose length is larger than the
337 3-D sliding mass length. It is also interesting to find that the location (i.e., 19.5m $\leq z \leq$ 42.5m)
338 where 2-D *FS* values are smaller than the 3-D *FS* is comparable with the sliding location (i.e.,
339 19.5m $\leq z \leq$ 43.5m) in 3-D slope stability analysis in this example, as shown in Fig. 7(b).
340 Although 2-D analysis could be more conservative than 3-D analysis based on the cross
341 section with minimal 2-D *FS*, the location of the 3-D critical slip surface remains unknown if
342 the 3-D analysis is not performed. Similar discussion can also be found in Griffiths and
343 Marquez (2008). Compared with 2-D slope probabilistic analysis, 3-D slope probabilistic
344 analysis can properly consider horizontal spatial variability in both lateral and axial directions,
345 and automatically locate the critical slip surface with the help of FE analysis. They are crucial
346 to slope risk assessment as illustrated in the following subsections.

347 **6.2 Reliability analysis and risk assessment using ARFEM**

348 To estimate the P_f and R for the slope example, one ARFEM run is performed with $m = 4$, N
349 $= 500$, and $p_0 = 0.1$ in preliminary analysis using the coarse FE model (i.e., Fig. 6(a)) and N_s
350 $= 25$ in target analysis using the fine FE model (i.e., Fig. 6(c)).

351 Table 1 summarizes the results of P_f and R for $fs = 1$. In preliminary analysis, the sample
352 space is divided into five subsets Ω_k, $k = 0, 1, \ldots, 4$, in a descending order of FS_p values
353 evaluated using the coarse FE model. These subsets contain 450, 450, 450, 450, and 50
354 random samples, respectively. Among them, 392 samples in Ω_3 and 50 samples in Ω_4 are

identified as failure samples for fs = 1. Based on these failure samples and their sliding mass volumes, $P_{f,p}$ and R_p are estimated as 8.84×10^{-4} and 1.77m^3, respectively. The preliminary analysis with 1850 coarse FE analyses requires about 7 hours by parallel computing on a desktop computer with 8 GB RAM and one Intel Core i7 CPU clocked at 3.4 GHz. Twenty five samples in each subset are then randomly selected for target analysis. As shown in Table 1, using the fine FE model, the target failure probabilities in Ω_2 and Ω_3 are refined from 0/450 and 392/450 to 5/25 and 25/25, respectively. The values of $P_{f,t}$ and R_t are refined as 2.80×10^{-3} and 7.09m^3, respectively, which are almost three and four times larger than the preliminary estimates (i.e., 8.84×10^{-4} and 1.77 m^3), respectively. Although only 125 fine FE analyses are performed in target analysis, its computational time (about 27 hours on the same computer using parallel computing) is much longer than that for preliminary analysis. In total, approximate 34 hours (or 1.4 days) is required using ARFEM for the slope example.

Figure 8 shows the variation of P_f and R with fs (i.e., CDF and CRF) obtained from the preliminary and target analyses in ARFEM. For all fs values, both P_f and R obtained from preliminary analysis are underestimated, as predicted in deterministic slope stability analysis. Hence only using coarse FE model in RFEM will lead to unconservative design of slopes. The shape of CRF is quite similar to that of CDF for the slope example. This indicates that the average consequence of slope failure (i.e., $\overline{C} = R/P_f$) is relatively insensitive to slope safety level (i.e., fs) compared with P_f and R. The observation is consistent with that in 2-D slope risk assessment (Li et al., 2016a).

6.3 Comparison between ARFEM and MCS-based RFEM

To validate the results obtained from ARFEM, a direct MCS-based RFEM run with 10,000 samples is carried out to calculate the P_f and R of the considered slope, where the fine FE model is directly used to perform deterministic slope stability analysis. The estimates of P_f and R are 3.20×10^{-3} and 7.00m^3, respectively, as shown in Table 2. These results agree with those (i.e., 2.80×10^{-3} and 7.09m^3) obtained from the target analysis in ARFEM because the same FE model is adopted. For comparison, Fig. 8 also shows the CDF and CRF obtained from MCS-based RFEM, which coincide with the target results of ARFEM for all *fs* values. These results indicate that ARFEM can produce consistent estimates of P_f and R compared with MCS-based RFEM.

Recall that only 125 fine FE analyses are required in ARFEM, which is much smaller than that (i.e., 10,000) required in MCS-based RFEM. Since the computational effort ratio ξ is about 1/50 on average, the equivalent sample size N_T of ARFEM calculated by Eq. (8) is 1850/50+125 = 162. In addition to the sample size, the COV of P_f is about $\sqrt{\left(1-P_f\right)/N_T P_f}$ = 0.18 for MCS-based RFEM. Using 20 independent runs, the COV of P_f from ARFEM is about 0.31. To achieve a fair comparison of the computational efficiency, the unit COV (Au, 2007) is taken as a measure of the computational efficiency in this study, which is defined as COV(P_f)$\times\sqrt{N_T}$ and accounts for the effect of number of samples used in simulation on the variation of reliability estimate. As shown in Table 2, the unit COV values of MCS-based RFEM and ARFEM are 18 and 3.9, respectively. In other words, ARFEM only requires about 1/21 (i.e., $(3.9/18)^2$) of the computational effort for MCS-based RFEM to achieve the same computational accuracy. Physically, MCS-based RFEM takes about 89.9 days (about 3

397 months) to produce sufficiently accurate results on the same computer using parallel
398 computing. The computational cost is too high for practitioners. In contrast, the total
399 computational time of ARFEM is only about 1.4 days, acceptable for 3-D FE-based reliability
400 analysis in practice. ARFEM significantly improves the computational efficiency of 3-D
401 slope reliability analysis and risk assessment by incorporating the information obtained from
402 preliminary analysis with coarse FE model into target analysis with fine FE model.

403 **6.4 Correlation between coarse and fine FE models**

404 Figure 9 compares the *FS*, *V* and *L* of the selected 125 representative samples calculated by
405 both coarse and fine FE models in Subsection 6.2, and illustrates the 1:1 lines and respective
406 linear regression lines for reference. Although the linear regression lines do not overlap with
407 the 1:1 lines, these FE responses are well correlated. The high correlations indicate that the
408 coarse FE model used in preliminary analysis is appropriate and can reflect the main features,
409 particularly the *FS*, of the fine FE model well. In addition, similar to deterministic slope
410 stability analysis again, using coarse FE model generally leads to overestimation of *FS* and
411 underestimation of *V* and *L*, which subsequently results in the underestimation of P_f and *R*.
412 Such differences become more significant as responses increase.

413 **7 Effect of horizontal spatial variability on 3-D slope reliability and risk**

414 With the aid of the improved computational efficiency provided by ARFEM, this section
415 carries out a sensitivity study to explore the effect of horizontal spatial variability on 3-D
416 slope reliability and risk. Five values of horizontal autocorrelation distance (i.e., l_h = 10m,
417 20m, 40m, 80m, and 120m) are considered and the vertical autocorrelation distance l_v is taken

418 as 2m. For simplicity, all results presented in this section are obtained from target analysis in
419 ARFEM.

420 Figure 10(a) shows the slope failure probability and risk for different values of
421 normalized horizontal autocorrelation distance (i.e., l_h/B). When l_h/B increases from 0.1 to 1.2,
422 namely, the horizontal spatial variability becomes weaker, the estimated P_f and R
423 significantly increase by about two and three orders of magnitude, respectively. The influence
424 weakens when the horizontal autocorrelation distance exceeds half of the slope length (e.g.,
425 l_h/B = 0.8 and 1.2). Since the range of l_h is generally within 20m ~ 40m, horizontal spatial
426 variability will significantly affect P_f and R for long slopes, for instance, several kilometers
427 long levees.

428 With respect to slope failure mechanisms, the average sliding mass volume $\bar{V}$ and
429 average sliding mass length $\bar{L}$, evaluated by Eq. (5a) and failure samples, are shown in Fig.
430 10(b). As l_h/B increases from 0.1 to 1.2, $\bar{V}$ and $\bar{L}$ increase slightly in comparison with P_f
431 and R. Note that $\bar{V}$ is equivalent to the average failure consequence $\bar{C}$ in this study. It can
432 be concluded that R (i.e., $P_f \times \bar{C}$) is more sensitive to P_f than $\bar{C}$, similar to previous
433 observation in 2-D slope risk assessment (Li et al., 2016a). Additionally, $\bar{V}$ and $\bar{L}$ follow
434 similar trends as l_h/B increases. This makes the average sliding mass area on the cross section
435 (i.e., $E(V/L)$), which should be dominated by the lateral spatial variability, remain roughly
436 unchanged. Thus, the horizontal spatial variability in the axial direction, instead of that in the
437 lateral direction, affects 3-D slope failure mechanisms and average failure consequence.

438 Figure 11 shows the effects of horizontal spatial variability on the mean and COV values

of FS, V and L, which are evaluated using Eq. (5) and all random samples. As shown in Fig. 11(a), both mean and COV values of FS increase with increasing l_h. The increase in COV of FS leads to the increase in P_f. Figures 11(b) and (c) show that both the mean values of V and L increase and their COV values decrease as l_h increases. This implies that the number of possible failure modes along the axial direction reduces as the horizontal spatial variability weakens. For the extreme case that l_h becomes infinite, the 3-D slope is homogenous in the axial direction and can be simplified as a 2-D slope if the slope is long enough. This brings about only a few slope failure modes caused by the vertical spatial variability. Consequently, the COV values of V and L are minimal, and the corresponding mean values approach the results of the deterministic slope stability analysis.

Based on the aforementioned results, the horizontal spatial variability in the axial direction affects the failure mode, reliability and risk of 3-D slopes significantly, particularly for long slopes with relatively small horizontal autocorrelation distances (e.g., below half of the slope length). Such effects are properly incorporated into 3-D slope reliability analysis and risk assessment by ARFEM.

8 Summary and conclusion

This paper proposed an auxiliary random finite element method (ARFEM) for efficient three-dimensional (3-D) slope reliability analysis and risk assessment, and explored the effect of horizontal spatial variability on 3-D slope reliability and risk. A 3-D soil slope example was investigated to demonstrate the validity of ARFEM, and those results were verified by Monte Carlo Simulation-based RFEM. Several conclusions can be drawn:

(1) The proposed ARFEM not only provides reasonably accurate estimates of slope failure probability and risk, but also significantly reduces the computational effort, particularly at small probability levels. This benefits from the fact that ARFEM incorporates the information generated from preliminary analysis based on a coarse finite-element (FE) model into target analysis based on a fine FE model using response conditioning method. This can significantly enhance the applications of RFEM in geotechnical practice.

(2) 3-D slope probabilistic analysis (including both 3-D slope stability analysis and 3-D spatial variability modeling of soil properties) can reflect slope failure mechanism more realistically in terms of the shape, location and length of slip surface. With the 3-D FE analysis of slope stability, ARFEM provides a rigorous tool for 3-D slope probabilistic analysis, where 3-D spatial variability of soil properties are explicitly modeled.

(3) Horizontal spatial variability, particularly in the axial direction, might significantly influence the failure mode, reliability and risk of 3-D slopes, especially for long slopes with relatively small horizontal autocorrelation distances (e.g., below half of the slope length). These effects can be properly incorporated into 3-D slope reliability analysis and risk assessment using ARFEM.

Although the coarse and fine FE models used in this study differ in their mesh size only, the proposed method applies generally to a coarse FE model with simplified soil constitutive model, large time-step, or any other techniques to improve the efficiency of deterministic FE analysis.

Acknowledgments

This work was supported by the National Science Fund for Distinguished Young Scholars (Project No. 51225903), the National Natural Science Foundation of China (Project Nos. 51329901, 51579190, 51528901), and the Natural Science Foundation of Hubei Province of China (Project No. 2014CFA001).

References

Ang, A. H-S., Tang, W. H. (2007). Probability concepts in engineering: emphasis on applications to civil and environmental engineering (2nd edition). Hoboken, New Jersey: John Wiley & Sons.

Au, S. K. (2007). Augmenting approximate solutions for consistent reliability analysis. Probabilistic Engineering Mechanics, 22(1), 77-87.

Au, S. K., Beck, J. L. (2001). Estimation of small failure probabilities in high dimensions by Subset Simulation. Probabilistic Engineering Mechanics, 16(4), 263-277.

Au, S. K., Wang, Y. (2014). Engineering risk assessment with Subset Simulation. Singapore: John Wiley & Sons.

Cao, Z., Wang, Y. (2014). Bayesian model comparison and selection of spatial correlation functions for soil parameters. Structural Safety, 49, 10-17.

Cao, Z., Wang, Y., Li, D. Q. (2016). Quantification of prior knowledge in geotechnical site characterization. Engineering Geology, 203, 107-116.

Chen, H. X., Zhang, S., Peng, M., Zhang, L. M. (2016). A physically-based multi-hazard risk assessment platform for regional rainfall-induced slope failures and debris flows. Engineering Geology, 203, 15-29.

Ching, J., Wang, J. S. (2016). Application of the transitional Markov chain Monte Carlo algorithm to probabilistic site characterization. Engineering Geology, 203, 151-167.

Dassault Systèmes. (2015). Abaqus Unified FEA, http://www.3ds.com/products-services/simulia/portfolio/abaqus/latest-release/.

Griffiths, D. V., Lane, P. A. (1999). Slope stability analysis by finite elements. Geotechnique, 49(3), 387-403.

Griffiths, D. V., Fenton, G. A. (2004). Probabilistic slope stability analysis by finite elements. Journal of Geotechnical and Geoenvironmental Engineering, 130(5), 507-518.

Griffiths, D. V., Marquez, R. M. (2007). Three-dimensional slope stability analysis by elasto-plastic finite elements. Geotechnique, 57(6), 537-546.

Griffiths, D. V., Marquez, R. M. (2008). Discussion: three-dimensional slope stability analysis by elasto-plastic finite elements. Geotechnique, 58(8), 683-685.

Griffiths, D. V., Huang, J., Fenton, G. A. (2009). On the reliability of earth slopes in three dimensions. Proceedings of the Royal Society of London A: Mathematical, Physical and Engineering Sciences, 465(2110), 3145-3164.

Hicks, M. A., Spencer, W. A. (2010). Influence of heterogeneity on the reliability and failure of a long 3D slope. Computers and Geotechnics, 37(7), 948-955.

Hicks, M. A., Nuttall, J. D., Chen, J. (2014). Influence of heterogeneity on 3D slope reliability and failure consequence. Computers and Geotechnics, 61, 198-208.

Huang, J., Lyamin, A. V., Griffiths, D. V., Krabbenhoft, K., Sloan, S. W. (2013). Quantitative risk assessment of landslide by limit analysis and random fields. Computers and

523 Geotechnics, 53, 60-67.
524 Jamshidi Chenari, R., Alaie, R. (2015). Effects of anisotropy in correlation structure on the
525 stability of an undrained clay slope. Georisk: Assessment and Management of Risk for
526 Engineered Systems and Geohazards, 2015, 9(2), 109-123.
527 Ji, J., Low, B. K. (2012). Stratified response surfaces for system probabilistic evaluation of
528 slopes. Journal of Geotechnical and Geoenvironmental Engineering, 138(11),
529 1398-1406.
530 Ji, J. (2014). A simplified approach for modelling spatial variability of undrained shear
531 strength in out-plane failure mode of earth embankment. Engineering Geology, 183,
532 315-323.
533 Ji, J., Chan, C. L. (2014). Long embankment failure accounting for longitudinal spatial
534 variation – A probabilistic study. Computers and Geotechnics, 61, 50-56.
535 Jiang, S. H., Li, D. Q., Cao, Z. J., Zhou, C. B., Phoon, K. K. (2015). Efficient system
536 reliability analysis of slope stability in spatially variable soils using Monte Carlo
537 Simulation. Journal of Geotechnical and Geoenvironmental Engineering, 141(2),
538 04014096.
539 Jiang, S. H., Li, D. Q., Zhang, L. M., Zhou, C. B. (2014). Slope reliability analysis
540 considering spatially variable shear strength parameters using a non-intrusive stochastic
541 finite element method. Engineering Geology, 168, 120-128.
542 Kasama, K., Whittle, A. J. (2016). Effect of spatial variability on the slope stability using
543 Random Field Numerical Limit Analyses. Georisk: Assessment and Management of

544 Risk for Engineered Systems and Geohazards, 10(1), 42-54.
545 Le, T. M. H. (2014). Reliability of heterogeneous slopes with cross-correlated shear strength
546 parameters. Georisk: Assessment and Management of Risk for Engineered Systems and
547 Geohazards, 8(4), 250-257.
548 Li, C. C., Der Kiureghian, A. (1993). Optimal discretization of random fields. Journal of
549 Engineering Mechanics, 119(6), 1136-1154.
550 Li, D., Chen, Y., Lu, W., Zhou, C. (2011). Stochastic response surface method for reliability
551 analysis of rock slopes involving correlated non-normal variables. Computers and
552 Geotechnics, 38(1), 58-68.
553 Li, D. Q., Qi, X. H., Phoon, K. K., Zhang, L. M., Zhou, C. B. (2014a). Effect of spatially
554 variable shear strength parameters with linearly increasing mean trend on reliability of
555 infinite slopes. Structural Safety, 49, 45-55.
556 Li, D. Q., Jiang, S. H., Cao, Z. J., Zhou, W., Zhou, C. B., Zhang, L. M. (2015a). A multiple
557 response-surface method for slope reliability analysis considering spatial variability of
558 soil properties. Engineering Geology, 187, 60-72.
559 Li, D. Q., Zhang, L., Tang, X. S., Zhou, W., Li, J. H., Zhou, C. B., Phoon, K. K. (2015c).
560 Bivariate distribution of shear strength parameters using copulas and its impact on
561 geotechnical system reliability. Computers and Geotechnics, 68, 184-195.
562 Li, D. Q., Xiao, T., Cao, Z. J., Zhou, C. B., Zhang, L. M. (2016a). Enhancement of random
563 finite element method in reliability analysis and risk assessment of soil slopes using
564 Subset Simulation. Landslides, 13: 293-303.

565 Li, D. Q., Xiao, T., Cao, Z. J., Phoon, K. K., Zhou, C. B. (2016b). Efficient and consistent
566 reliability analysis of soil slope stability using both limit equilibrium analysis and finite
567 element analysis. Applied Mathematical Modelling, 40(9-10): 5216-5229.
568 Li, D. Q., Zheng, D., Cao, Z. J., Tang, X. S., Phoon, K. K. (2016c). Response surface
569 methods for slope reliability analysis: Review and comparison. Engineering Geology,
570 203, 3-14.
571 Li, D. Q., Qi, X. H., Cao, Z. J., Tang, X. S., Phoon, K. K., Zhou, C. B. (2016d). Evaluating
572 slope stability uncertainty using coupled Markov chain. Computers and Geotechnics, 73,
573 72-82.
574 Li, L., Wang, Y., Cao, Z. (2014b). Probabilistic slope stability analysis by risk aggregation.
575 Engineering Geology, 176, 57-65.
576 Li, Y. J., Hicks, M. A., Nuttall, J. D. (2015b). Comparative analyses of slope reliability in 3D.
577 Engineering Geology, 196, 12-23.
578 Lloret-Cabot, M., Fenton, G. A., Hicks, M. A. (2014). On the estimation of scale of
579 fluctuation in geostatistics. Georisk: Assessment and Management of Risk for
580 Engineered Systems and Geohazards, 8(2), 129-140.
581 Phoon, K. K., Kulhawy, F. H. (1999). Characterization of geotechnical variability. Canadian
582 Geotechnical Journal, 36(4), 612-624.
583 Phoon, K. K., Ching, J. Y. (2014). Risk and Reliability in Geotechnical Engineering.
584 Singapore: Taylor and Francis.
585 Pradlwarter, H. J., Schuëller, G. I. (2010). Local domain Monte Carlo Simulation. Structural

586 Safety, 32(5), 275-280.
587 Santoso, A. M., Phoon, K. K., Quek, S. T. (2011). Effects of soil spatial variability on
588 rainfall-induced landslides. Computers & Structures, 89(11), 893-900.
589 Sudret, B., Der Kiureghian, A. (2000). Stochastic finite element methods and reliability: a
590 state-of-the-art report. Department of Civil and Environmental Engineering, University
591 of California.
592 Schuëller, G. I., Pradlwarter, H. J., Koutsourelakis, P. S. (2004). A critical appraisal of
593 reliability estimation procedures for high dimensions. Probabilistic Engineering
594 Mechanics, 19(4), 463-474.
595 Tang, X. S., Li, D. Q., Rong, G., Phoon, K. K., Zhou, C. B. (2013). Impact of copula
596 selection on geotechnical reliability under incomplete probability information.
597 Computers and Geotechnics, 49, 264-278.
598 Tang, X. S., Li, D. Q., Zhou, C. B., Phoon, K. K. (2015). Copula-based approaches for
599 evaluating slope reliability under incomplete probability information. Structural Safety,
600 52, 90-99.
601 Vanmarcke, E. H. (1977). Reliability of earth slopes. Journal of the Geotechnical Engineering
602 Division, 103(12), 1247-1265.
603 Vanmarcke, E. H. (2011). Risk of limit-equilibrium failure of long earth slopes: how it
604 depends on length. In Geotechnical Risk Assessment & Management (GeoRisk 2011),
605 Atlanta, Georgia, United States, June 26-28, 2011. pp. 1-24. DOI: 10.1061/41183(418)1.
606 Vanmarcke, E. H. (2010). Random fields: analysis and synthesis (revised and expanded new

607 edition). Singapore: World Scientific Publishing Co. Pte. Ltd.
608 Vorechovsky, M. (2008). Simulation of simply cross correlated random fields by series
609 expansion methods. Structural Safety, 30(4), 337-363.
610 Wang, Y., Cao, Z., Au, S. K. (2010). Efficient Monte Carlo simulation of parameter
611 sensitivity in probabilistic slope stability analysis. Computers and Geotechnics, 37(7),
612 1015-1022.
613 Wang, Y., Cao, Z., Au, S. K. (2011). Practical reliability analysis of slope stability by
614 advanced Monte Carlo Simulations in a spreadsheet. Canadian Geotechnical Journal,
615 48(1), 162-172.
616 Wang, Y., Cao, Z., Li, D. (2016). Bayesian perspective on geotechnical variability and site
617 characterization. Engineering Geology, 203, 117-125.
618 Xiao, T., Li, D. Q., Cao, Z. J., Tang, X. S. (2015). Non-intrusive reliability analysis of
619 multi-layered slopes in spatially variable soils. In fifth International Symposium on
620 Geotechnical Safety and Risk (ISGSR 2015), Rotterdam, The Netherlands, October
621 13-16, 2015. Geotechnical Safety and Risk V, Schweckendiek, T. et al. (Eds.), pp
622 184-190.
623 Zhu, H., Zhang, L. M., Zhang, L. L., Zhou, C. B. (2013). Two-dimensional probabilistic
624 infiltration analysis with a spatially varying permeability function. Computers and
625 Geotechnics, 48, 249-259.
626

List of Figures

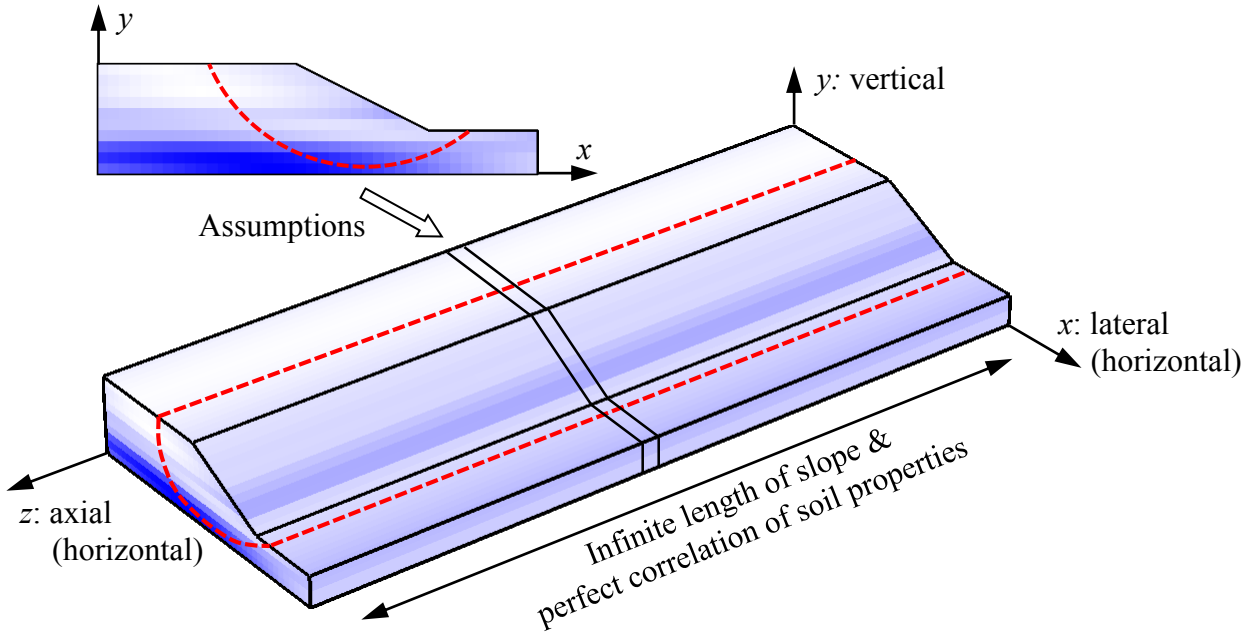

Fig. 1 Assumptions made in 2-D slope reliability analysis

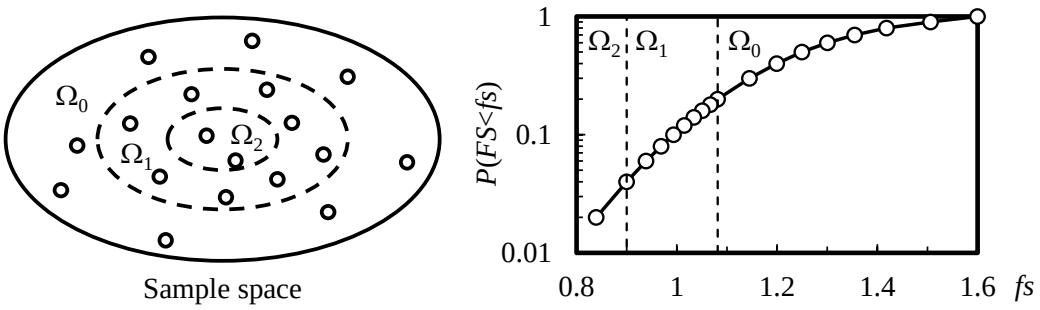

(a) SS using coarse FE model

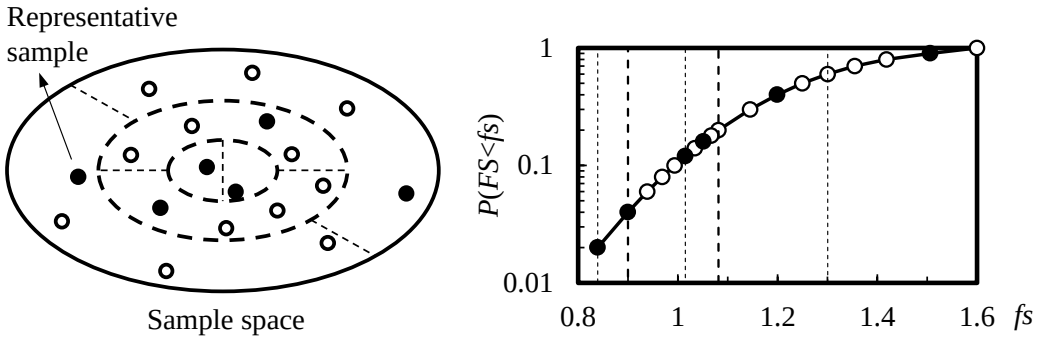

(b) Sub-binning and selection of representative samples in each subset

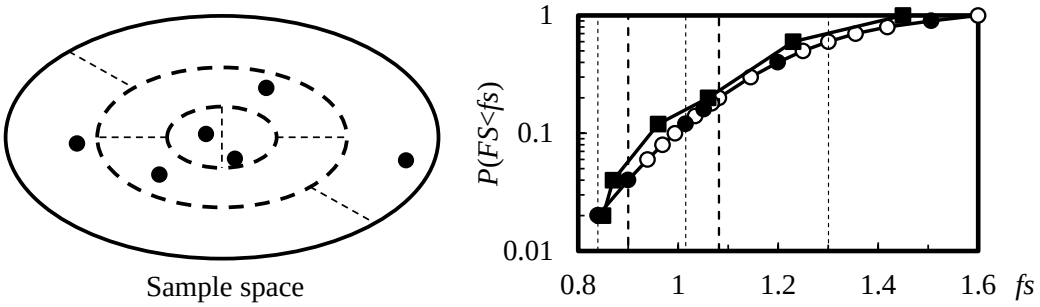

(c) RCM using fine FE model

Fig. 2 Schematic diagram of SS and RCM ($N = 10$, $p_0 = 0.2$, $m = 2$, $N_s = 2$) (modified from Li et al. (2016b))

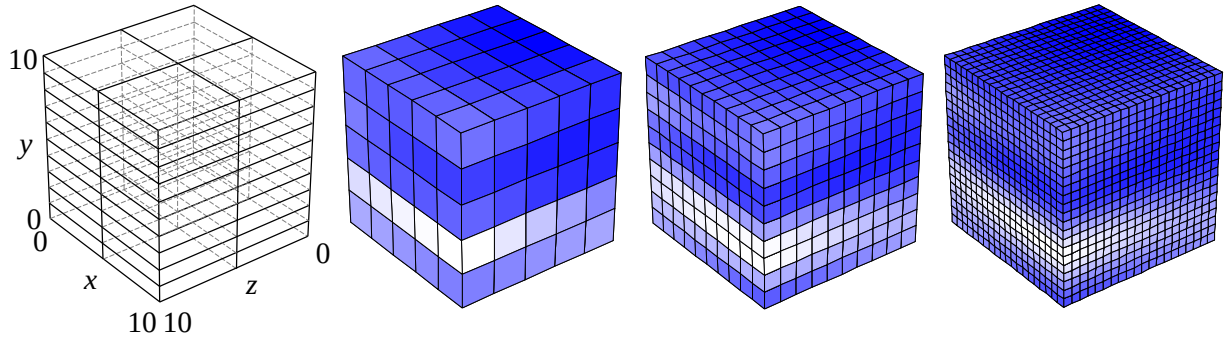

(a) Random field grid (l_h = 10m, l_v = 2m)

(b) FE mesh I (mesh size = 2m)

(c) FE mesh II (mesh size = 1m)

(d) FE mesh III (mesh size = 0.5m)

Fig. 3 Identical random field realization mapped onto different FE meshes using EOLE

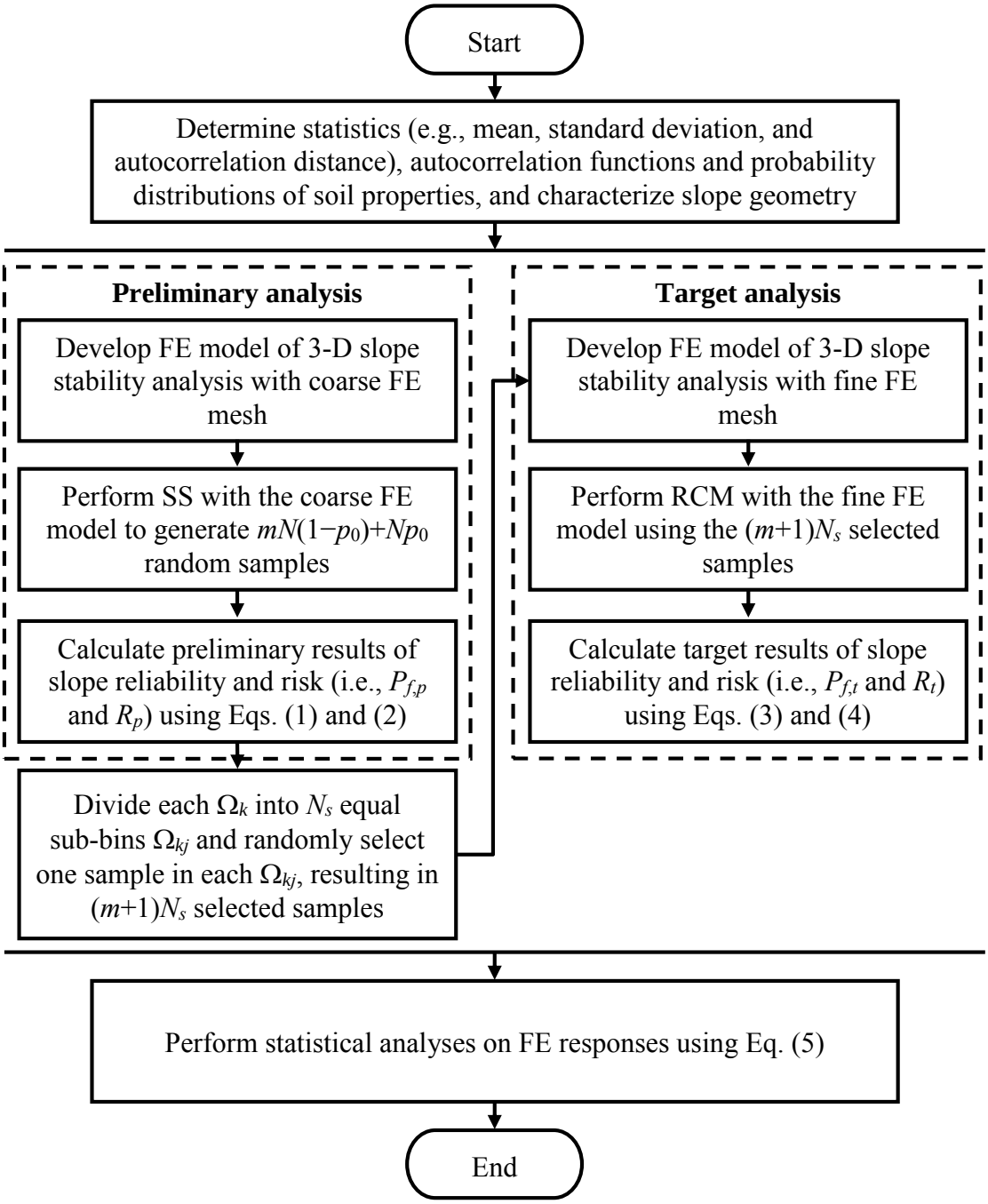

Fig. 4 Implementation procedure of ARFEM for 3-D slope reliability and risk assessment

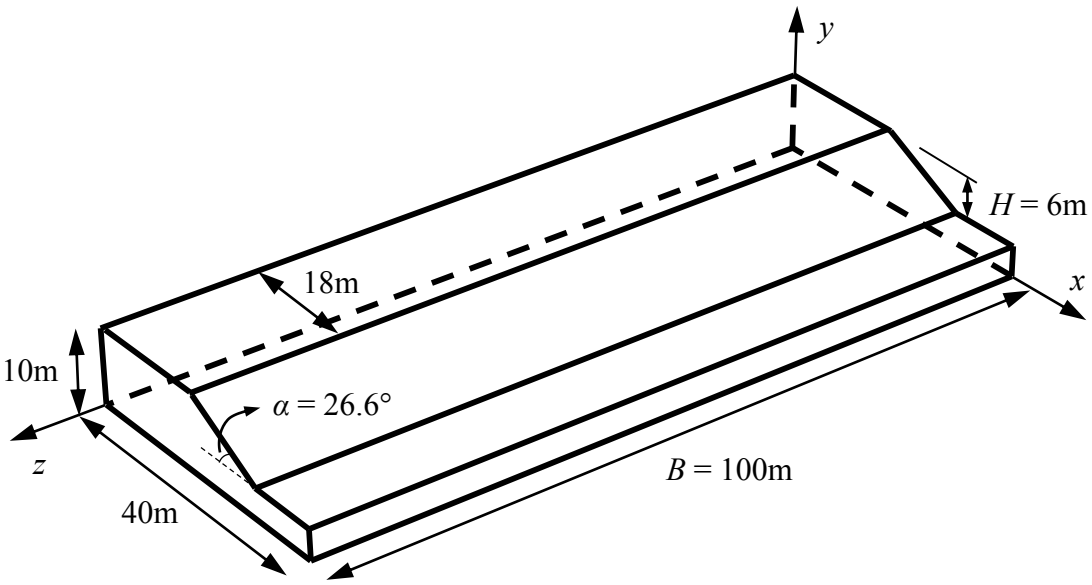

Fig. 5 Geometry of slope example

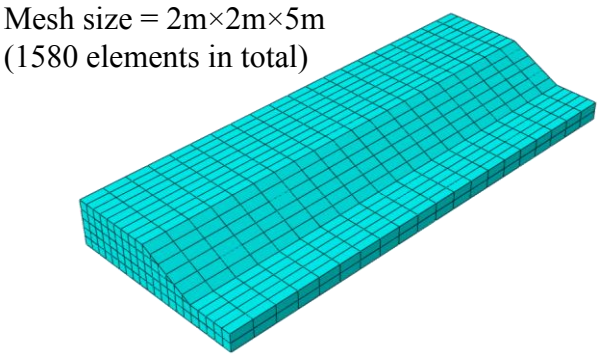

(a) FE mesh for coarse FE model

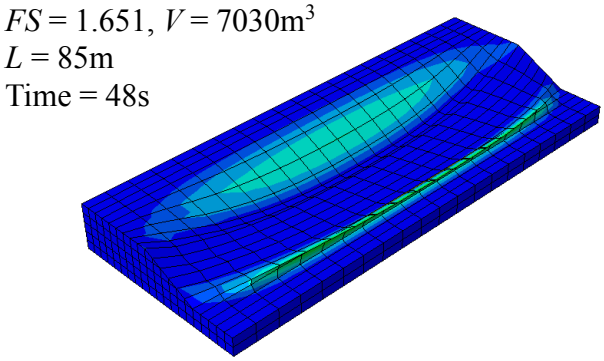

(b) Results using coarse FE model

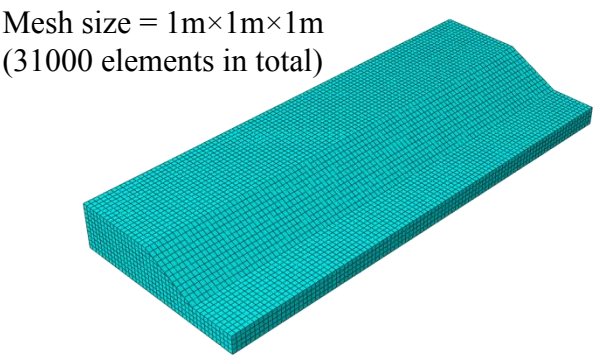

(c) FE mesh for fine FE model

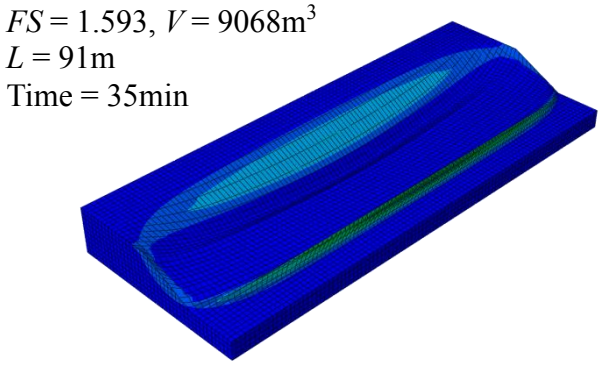

(d) Results using fine FE model

Fig. 6 Coarse and fine FE models and deterministic analysis results

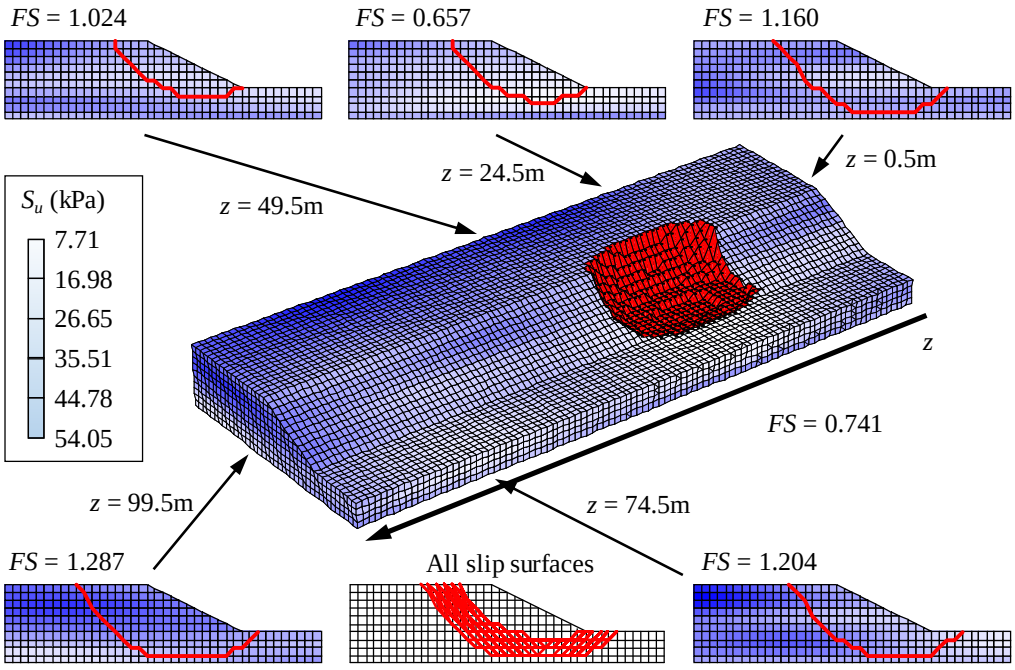

(a) Slip surfaces for 2-D and 3-D analyses

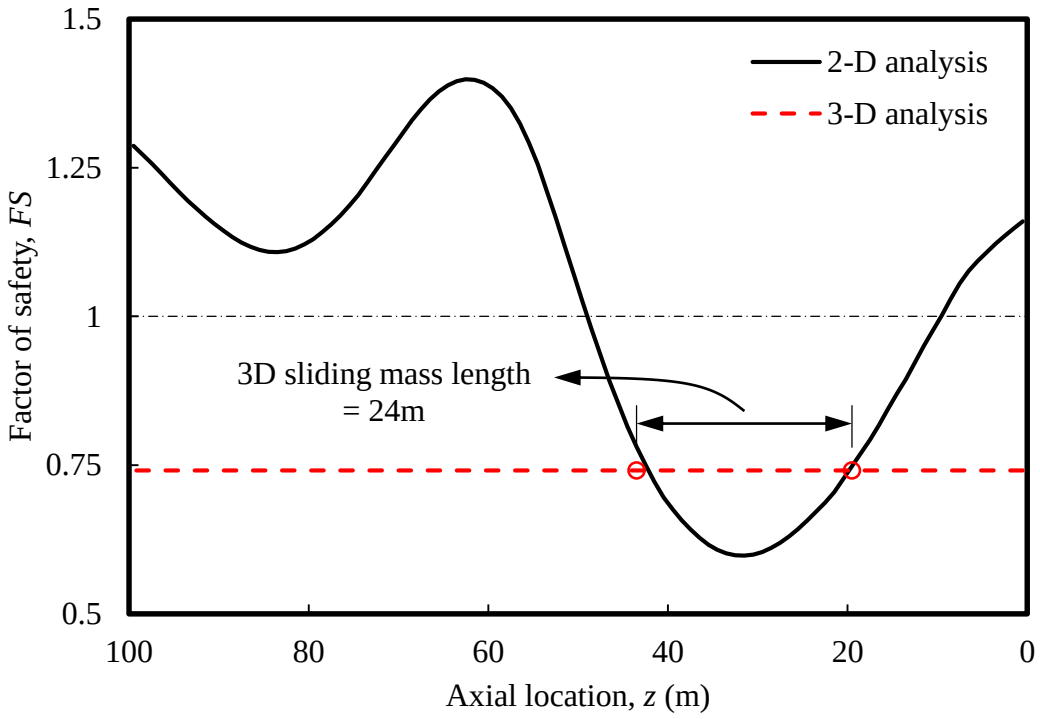

(b) Factor of safety for 2-D and 3-D analyses

Fig. 7 Results of 2-D and 3-D analyses for a typical random field realization

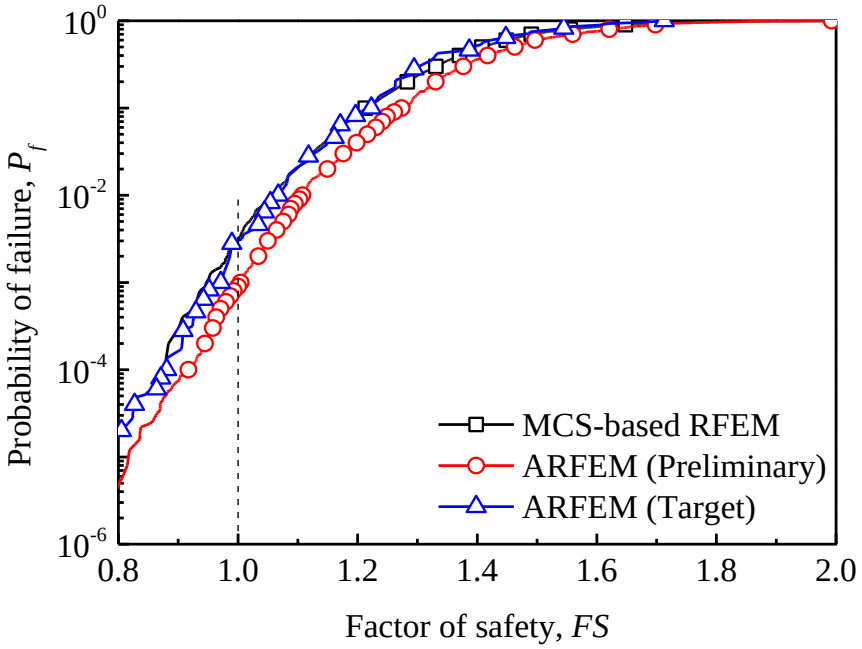

(a) Cumulative distribution function (CDF)

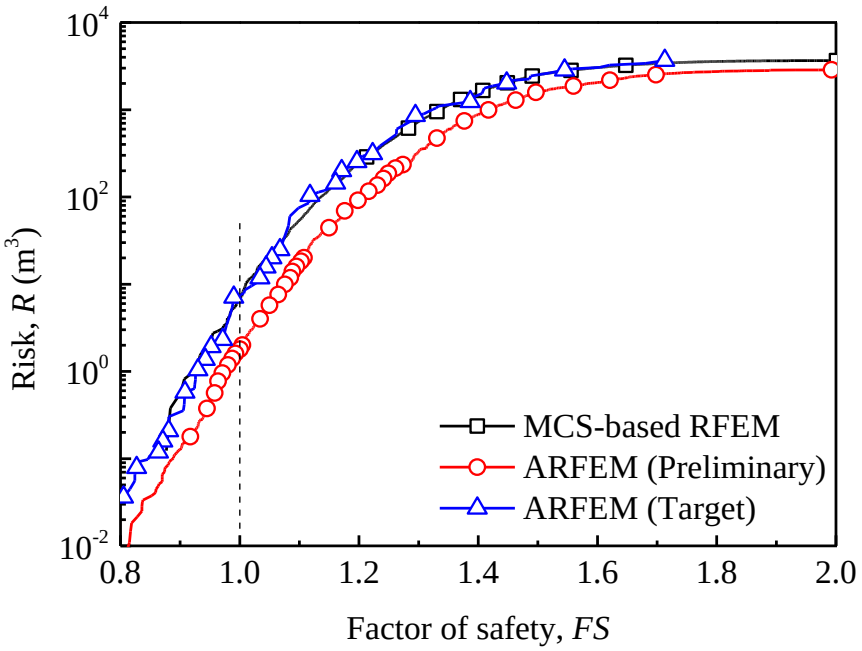

(b) Cumulative risk function (CRF)

Fig. 8 CDFs and CRFs obtained from MCS-based RFEM and ARFEM

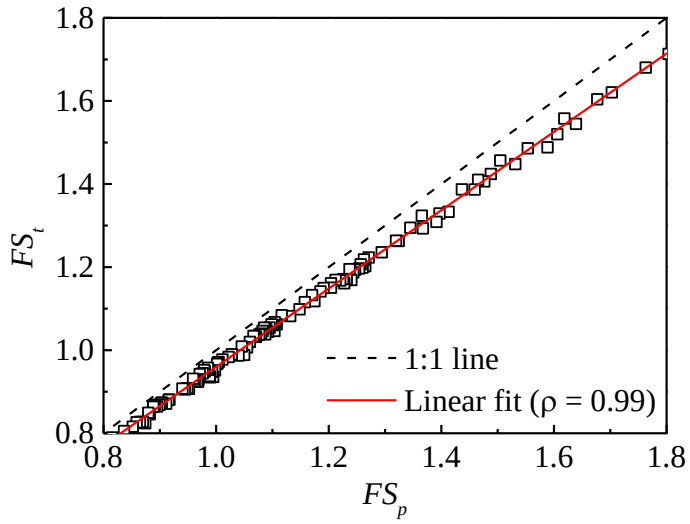

(a) Factor of safety, *FS*

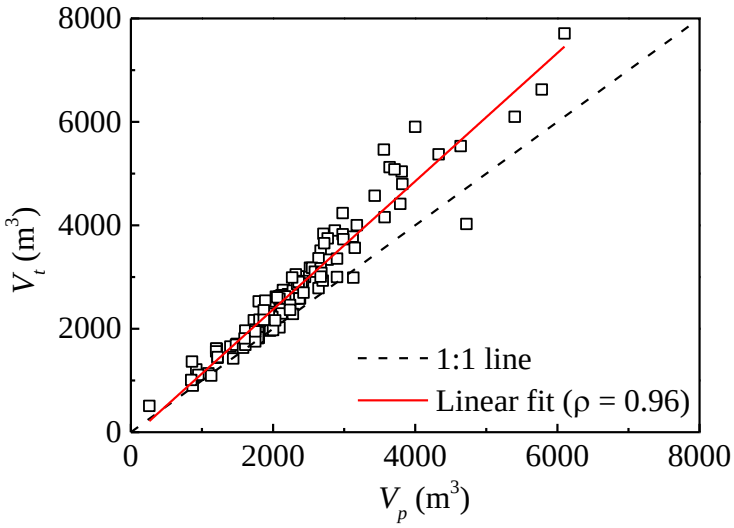

(b) Sliding mass volume, *V*

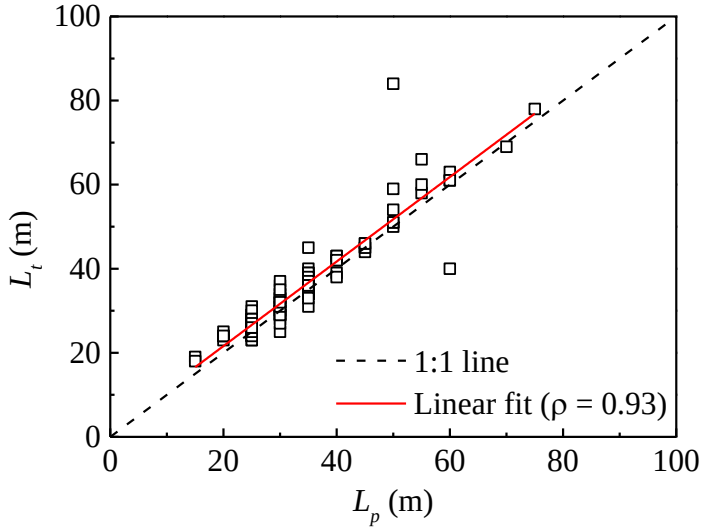

(c) Sliding mass length, *L*

Fig. 9 Comparison of FE responses obtained from coarse and fine FE models

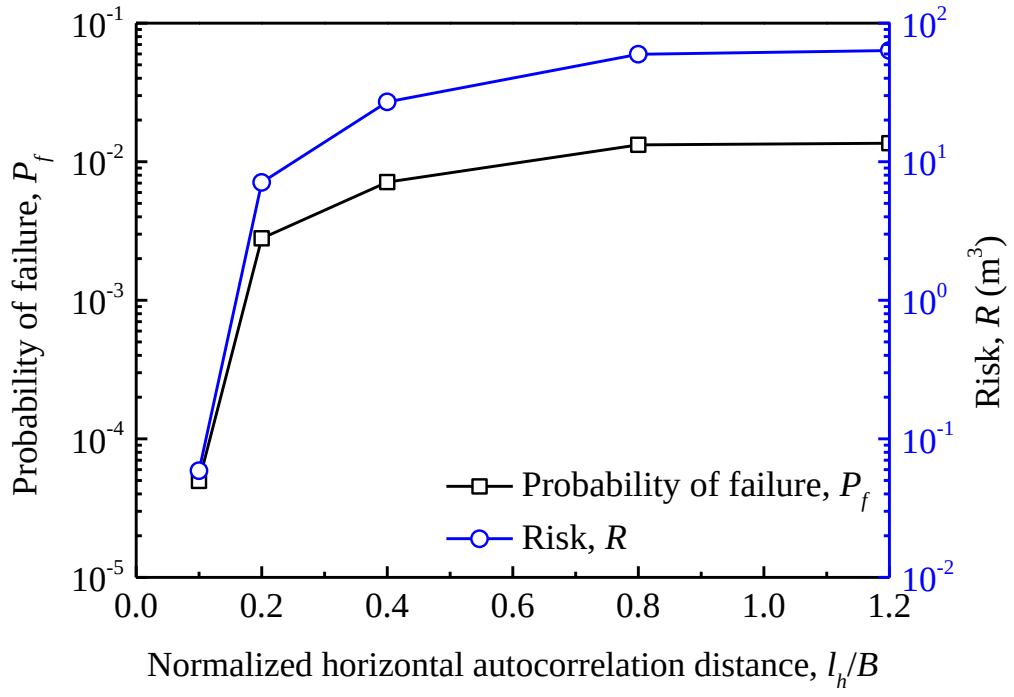

(a) Slope failure probability and risk

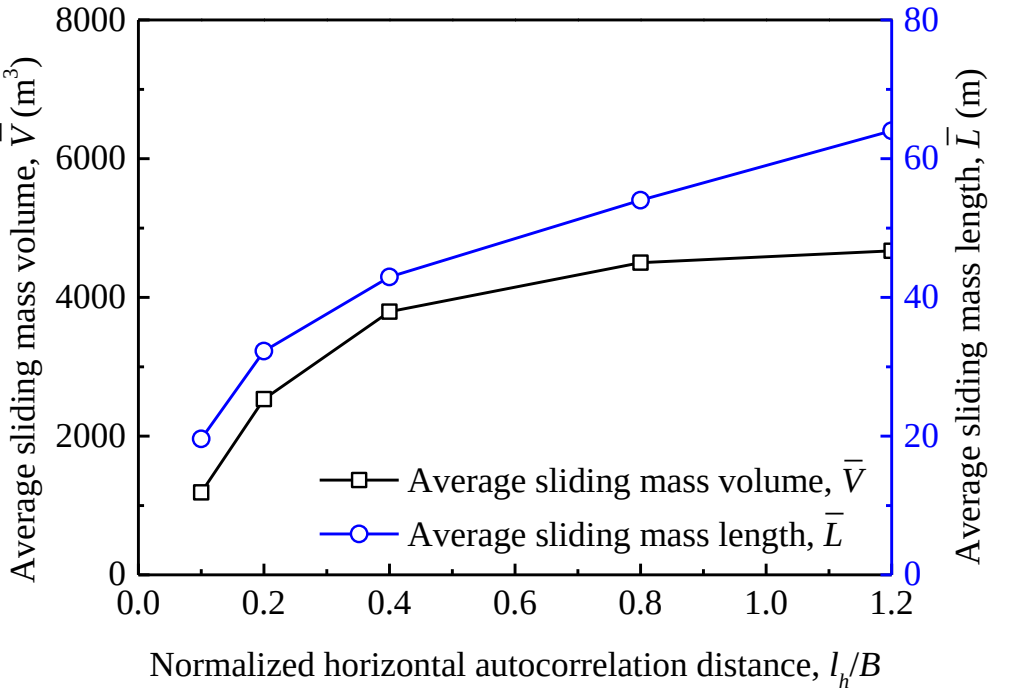

(b) Average sliding mass volume and length

Fig. 10 Effect of horizontal spatial variability on results of slope failure

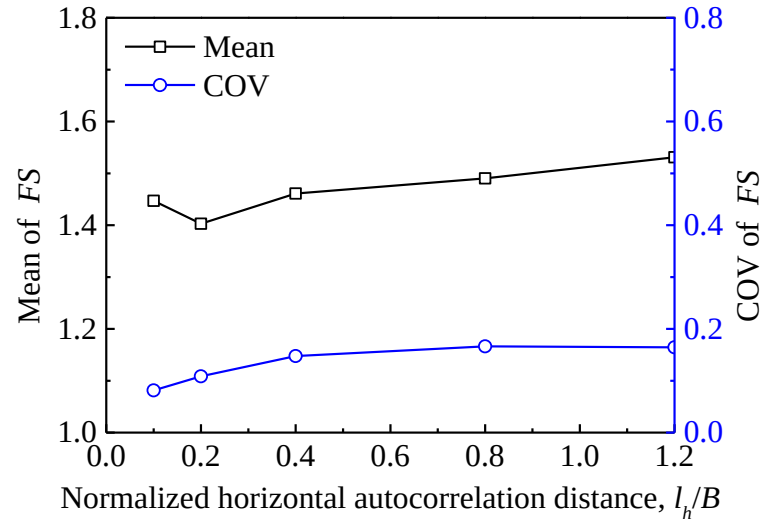

(a) Factor of safety, *FS*

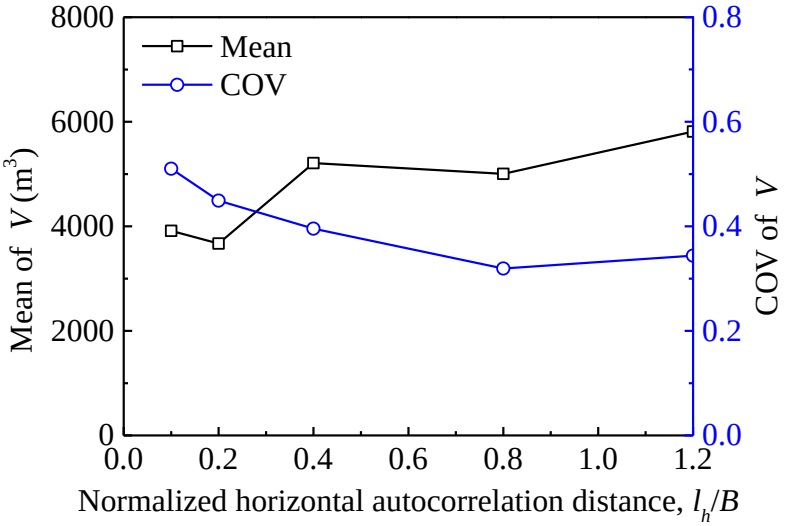

(b) Sliding mass volume, *V*

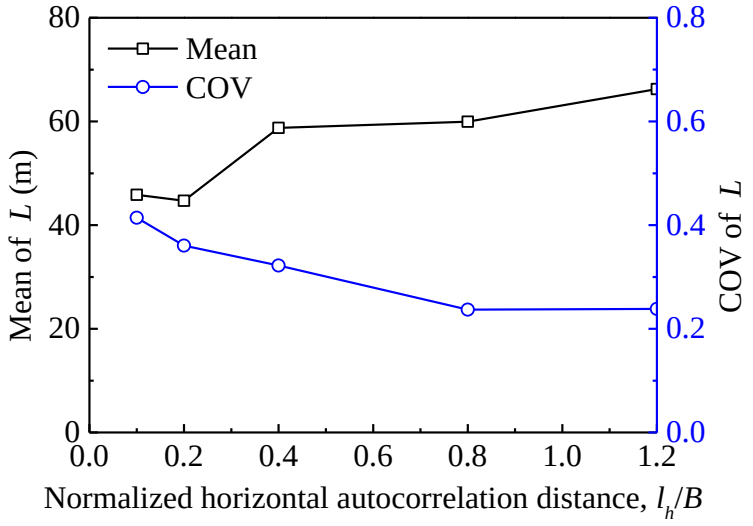

(c) Sliding mass length, *L*

Fig. 11 Effect of horizontal spatial variability on FE responses of slope

List of Tables

Table 1. Results of slope reliability and risk assessment using ARFEM

k	Ω_k	$P(\Omega_k)$	Preliminary analysis			Target analysis		
			$P(F_p\|\Omega_k)$	$P_{f,p}$	R_p (m^3)	$P(F_t\|\Omega_k)$	$P_{f,t}$	R_t (m^3)
0	$1.274 \le FS_p$	9×10^{-1}	0/450			0/25		
1	$1.109 \le FS_p < 1.274$	9×10^{-2}	0/450			0/25		
2	$1.005 \le FS_p < 1.109$	9×10^{-3}	0/450	8.84×10^{-4}	1.77	5/25	2.80×10^{-3}	7.09
3	$0.917 \le FS_p < 1.005$	9×10^{-4}	392/450			25/25		
4	$FS_p < 0.917$	1×10^{-4}	50/50			25/25		

Table 2. Comparison of results between MCS-based RFEM and ARFEM

Method		N_T	Time (d)[a]	P_f	COV(P_f)	R (m^3)	Unit COV
MCS-based RFEM		10000	89.9	3.20×10^{-3}	0.18	7.00	18
ARFEM	Preliminary	1850	0.3[c]				
			162[b]	1.4[c]	2.80×10^{-3} [c]	0.31[c]	6.71[c]	3.9
	Target	125	1.1[c]				

Note: [a] Estimated by parallel computing; [b] $\xi \approx 1/50$ on average; [c] Estimated on 20 independent runs.